University of Oxford, St. Anne's College

2011

12th Oxford Summer School on Neutron Scattering

Answer Book

5th – 16th September 2011

http://www.oxfordneutronschool.org

A. Single-Crystal Diffraction

A1.

(i) From the relation $\lambda = h/(m_n v_n)$ we get

$$\lambda \text{ (Å)}=3.956/v_n\,(km/\text{sec}).$$

Putting $v_n = 2.20$ *km/sec* gives $\lambda = \underline{\textbf{1.798 Å}}$.

(ii) Similarly from $E = \dfrac{1}{2} m_n v_n^2$ we obtain $E = \underline{\textbf{25.30 \textit{meV}}}$.

(iii) The X-ray energy is given by:

$$E_X = h\nu = \frac{hc}{\lambda}$$

with ν the frequency of the X-rays and c the velocity of light.
Putting $c = 2.998x10^8\,m/\text{sec}$ and $\lambda = 1.8x10^{-10}\,m$ gives

$$E = \underline{\textbf{6.88 kV}}$$

(iv) The velocity of a neutron with this energy is

$$v_n = \left(\frac{2E}{m_n}\right)^{1/2},$$

i.e. $v_n = \underline{\textbf{1148\textit{km/sec}}}$

We see then that thermal neutrons have both wavelengths suitable for studying atomic structures in the 1-100Å range and energies suitable for studying excitations (such as phonons or magnons) in the meV-eV range. (Fast neutrons have too short a wavelength and are too energetic for either purpose.)

A2

(i). The wavelength of the reflected beam is

$$\lambda = 2d_{111}\sin\theta$$

where $d_{111} = \dfrac{a_0}{\sqrt{3}} = 2.85\,\mathring{A}$. Thus $\sin\theta = 1.8/5.7$ and the scattering angle is

$$2\theta = \underline{\mathbf{36.7}} \; ^{\circ}.$$

(ii). The wavelength spread is derived by differentiating Bragg's equation:

$$\frac{\Delta\lambda}{\lambda} = -\cot\theta.\Delta\theta \; .$$

Putting $\Delta\theta = 0.2^{\circ}$ gives $\dfrac{\Delta\lambda}{\lambda} = 0.0105$, so that for $\lambda = 1.8\,\mathring{A}$ we get

$$\Delta\lambda = \underline{\pm\mathbf{0.019}\mathring{A}}$$

Note that this spread of wavelengths is much larger than the natural width of characteristic X-ray lines, and so Bragg peaks obtained with neutrons will not be as sharp as X-ray peaks.

A3

Figure A1 shows the reciprocal lattice in the $\mathbf{a}^*\mathbf{b}^*$ plane, together with the Ewald circles passing through the reflections *630* and *360* .
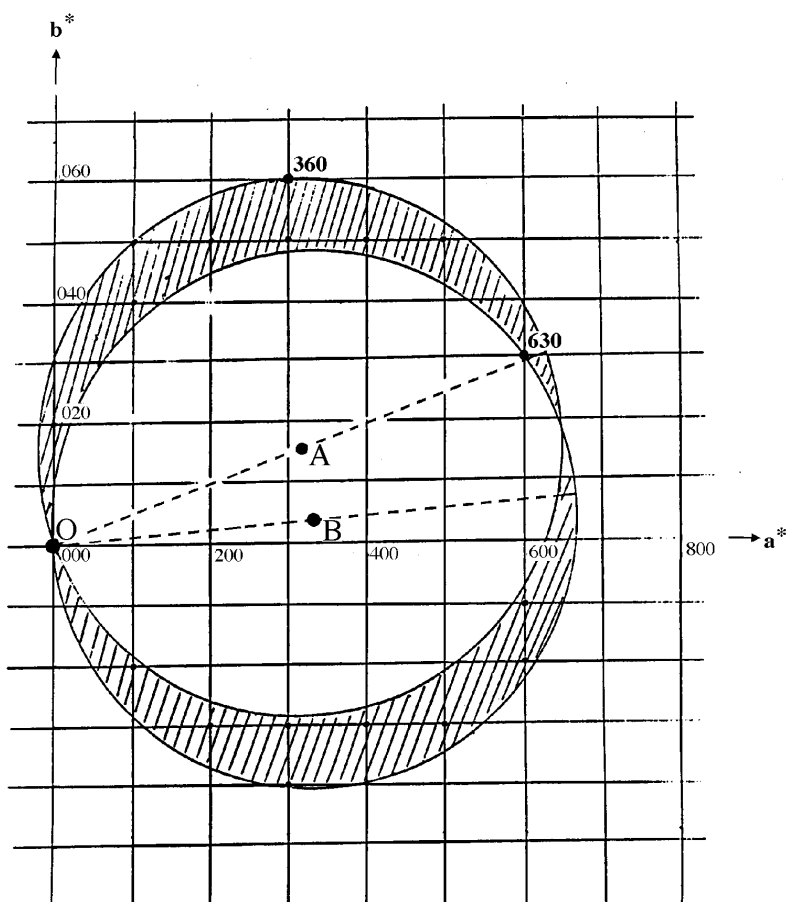

Figure A1. *The Ewald circles for the 630 and 360 reflections. A is the centre of the circle for 360 and B is the centre of the circle for 630.*

We can consider the crystal to be stationary and the incident beam to turn between the directions $\mathbf{AO}\rightarrow$ and $\mathbf{BO}\rightarrow$ in the Figure. During this rotation the area swept out in reciprocal space is the shaded region. The number of reciprocal lattice points in this region, i.e. the number of Bragg reflections, is approximately 18.

A4

Figure A2 shows the Ewald circles drawn for the two extreme wavelengths. The observable reflections are those lying in the shaded area lying between the two circles. For a primitive unit cell there are no

3

systematically absent reflections, and so the number of possible reflections is about sixty.
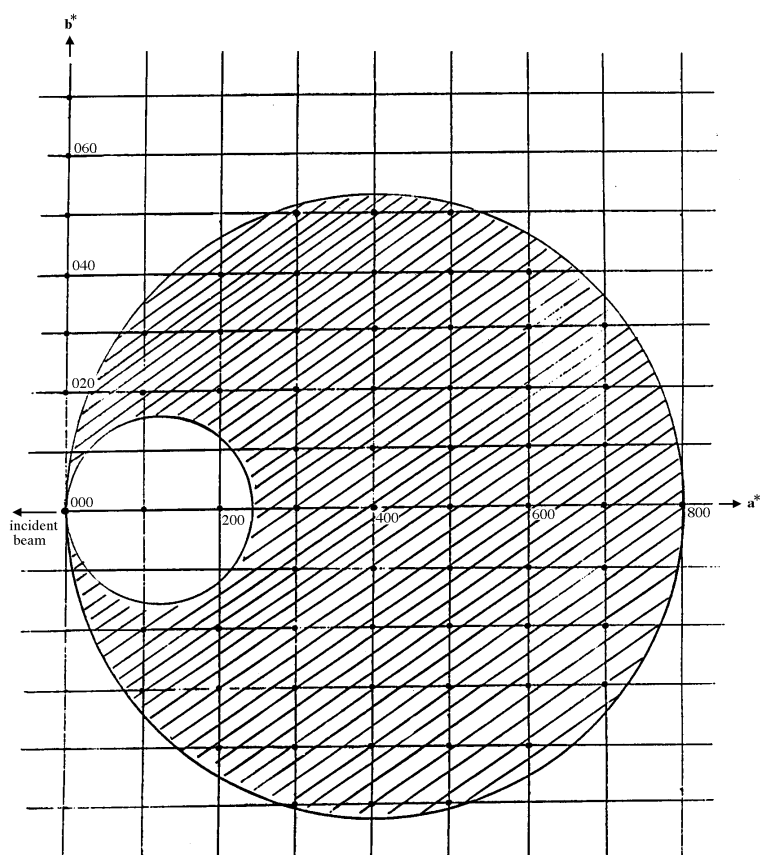

Figure A2. *The Ewald construction showing the reflection circles for the minimum wavelength (maximum radius) and the maximum wavelength (minimum radius).*

B. Coherence and Incoherence

B1

(1) <u>Hydrogen</u>. b_{coh} is derived by averaging the scattering length over the states with parallel and antiparallel neutron–nucleus spin states, Eq. (B2),

The weights are given by Eq. (B1): $w^+ = (I+1)/(2I+1)$ and $w^- = I/(2I+1)$. Setting $I = \frac{1}{2}$ we have $w^+ = \frac{3}{4}$ and $w^- = \frac{1}{4}$. From Table B.1,

$$= -3.74 \text{ fm}$$

The coherent scattering cross section is given by Eq. (B3),

$$= 1.75 \text{ b} \quad (1 \text{ b} = 10^{-28} \text{ m}^2)$$

The total cross section is obtained by summing the weighted values of the spin states of the combined nucleus-neutron system, Eq. (B4):

$$= 81.7 \text{ b}$$

Finally, the incoherent scattering cross section is the difference between and

$$= 79.9 \text{ b}$$

(1) <u>Deuterium</u>. For $I = 1$ we have from Eq. (B1),   and   . From the data in Table B.1, and the formulae above,

$$b_{coh} = 6.67 \text{ fm}$$

$$\sigma_{coh} = 5.6 \text{ b}$$

5

$$\sigma_{tot} = 7.6 \text{ b}$$

$$\sigma_{inc} = 2.0 \text{ b}$$

B2

In this example the incoherent scattering is mainly isotopic in origin, but there is a small contribution from the spin.

The coherent scattering length is the weighted average of the scattering lengths of the different isotopes, Eq. (B2):

Using Table B.1a below we have:

$$b_{coh} = 10.34 \text{ fm}$$

The coherent scattering cross section is given by Eq. (B3),

$$= 13.43 \text{ b}$$

The total scattering cross section is given by Eq. (B4),

where,

⎯⎯   ⎯⎯

Hence, $\qquad\qquad\qquad\sigma_{tot} = 18.50 \text{ b}$

Finally, from Eq. (B5), $\qquad\qquad$, we find that

$$\sigma_{inc} = 5.09 \text{ b}$$

isotope, r	spin I_r	(fm)	(fm)	(b)	(b)
58	0	9.883	0	1.416	0
60	0	0.73	0	0.020	0
61	3/2	2.88	4.73	0.132	0.595
62	0	0.31	0	0.027	0
64	0	0.00	0	0.000	0

C. Time-of-Flight Powder Diffraction

C1.

(a) The expression

$$t = \left(\frac{m_n}{h}\right)\lambda L$$

follows from the relations

$$L = vt$$

$$\lambda = \frac{h}{m_n v}$$

where v is the neutron velocity.

From the values of h and m_n on page 2 we get

$$t(in\ \mu secs) = 252.8\lambda(in\ \text{Å})\ \text{x}\ L(in\ metres).$$ (C1a)

(b)   In Bragg scattering from lattice planes *hkl* of spacing d_{hkl} the wavelength of the scattered radiation is given by

$$\lambda = 2d_{hkl}\sin\theta$$ (C2a)

where 2θ is the scattering angle.

Putting $L = 100m$ into eqn. (C1a) and $\theta = 85°$ into eqn. (C2a) gives

$$t(\mu secs) = 5.036\times 10^4\ d_{hkl}(\text{Å})$$

(C3a)

Perovskite has a primitive cubic lattice, so that the first three Bragg reflections (corresponding to the longest times-of-flight) are *100, 110* and *111*. Also the d-spacing is related to the lattice constant a_0 by

$$d_{hkl} = \frac{a_0}{\sqrt{\left(h^2 + k^2 + l^2\right)}},$$

(C4a)

and so $d_{100} = 3.84\text{Å}$, $d_{110} = 2.72\text{Å}$ and $d_{111} = 2.22\text{Å}$. Substituting into eqn (C3a) we find that $t_{100} = 194m\sec$, $t_{110} = 137m\sec$ and $t_{111} = 112m\sec$.

(c) Combining eqns. (C3a) (C4a) gives:

$$t \propto \left(h^2 + k^2 + l^2\right)^{-1/2}.$$

(C5a)

C2.

(a) The *Structure Factor* F_{hkl}, or the amplitude of the scattering into the *hkl* Bragg reflection by the atoms in one unit cell, is given by:

$$F_{hkl} = \sum_{j=1}^{N} b_j \exp\left\{2\pi i\left(hx_j + ky_j + lz_j\right)\right\}.$$

(C6a)

Here b_j is the scattering length of the jth nucleus in the cell, $x_j\ y_j\ z_j$ are its fractional coordinates, and N is the total number of atoms in the cell.

In the diamond structure of silicon there is a basis of two silicon atoms at

0,0,0 *and* ¼,¼,¼

and this basis is distributed at each of the face-centred-cubic lattice points:

0, 0, 0;   ½, ½, 0;   ½, 0, ½;   0, ½, ½

Hence N=8 and the fractional coordinates are

0, 0, 0;   ½, ½, 0;   ½, 0, ½;   0, ½, ½   for *j*=1 to 4

and

9

¼, ¼, ¼ + (0, 0, 0;   ½, ½, 0;   ½, 0, ½;   0, ½, ½)   for j=5 to 8.

Inserting these coordinates into eqn. (C6a) gives:

$$F_{hkl} = b_j \left\{ 1 + \exp\left[\pi i(h+k)\right] + \exp\left[\pi i(h+l)\right] + \exp\left[\pi i(k+l)\right] \right\}$$
$$x \left\{ 1 + \exp\left[\pi i\left(\frac{h+k+l}{2}\right)\right] \right\}. \qquad\qquad (C7a)$$

If all indices are even integers the first bracket {} is equal to 4; similarly, if all indices are odd integers. If only one index is even, the first bracket {} is zero; similarly, if only one index is odd.

(b) A further restriction on the indices of the Bragg reflections is imposed by the second bracket {} in eqn. (C7a). If $\left(\frac{h+k+l}{2}\right)$ is even, this bracket is equal to 2; if $\left(\frac{h+k+l}{2}\right)$ is odd, the bracket is zero.

(c)

(i) The possible values of *hkl* for the f.c.c. lattice are shown in Table C.1a.

Table C.1a Sums of three squared integers/ Miller indices.

$h^2+k^2+l^2$ / hkl	$h^2+k^2+l^2$ / hkl	$h^2+k^2+l^2$ / hkl	$h^2+k^2+l^2$ / hkl	$h^2+k^2+l^2$ / hkl
1	11* 311	21	33	43* 533
2	12* 222	22	34	44* 622
3* 111	13	24* 422	35* 531	45
4* 200	14	25	36* 600/442	46
5	16* 400	26	37	48* 444
6	17	27* 511/333	38	49
8* 220	18	29	40* 620	50
9	19* 331	30	41	51* 711/551
10	20* 420	32* 440	42	52* 640

(ii) The forbidden reflections are: 200, 222, 420, 600, 442, 622, 640.

(iii) The overlapping reflections are: 511/333; 711/551.

(d) Putting $L = 14m$ into eqn. (C1a) and $\theta = 83.5°$ into eqn. (C2a) gives

$$t(\mu secs) = 7033 d_{hkl}(\text{Å}) \quad . \qquad\qquad (C5a)$$

and from eqns(C3a) and (C4a):

$$\frac{1}{t^2} \propto h^2 + k^2 + l^2 \quad . \qquad\qquad (C6a)$$

111 is the Bragg peak with the longest flight time. The next peak is *220* (*200* is forbidden). Thus *220* is peak no 1 in Figure C.1. Using the information in section (c) the remaining peaks are readily indexed (see Table C.1a below).

Using eqn. (C5a) we get the cell size of $a_0 = 5.4307\text{Å}$.

Table C.1a

peak number	time of flight ($\mu secs$)	indices *hkl*
1	13 503	220
2	11 515	311
3	9 549	400
4	8 760	331
5	7 796	422
6	7 351	511/333
7	6 753	440
8	6 455	531
9	6 038	620
10	5 823	533
11	5 512	444
12	5 348	711/551

D. Magnetic Elastic Scattering

D1.

The equation for a Gaussian is:
$$f(x) = \frac{1}{\sqrt{2\pi\sigma^2}} \exp\left(-\frac{x^2}{2\sigma^2}\right)$$

The Fourier transform of this Gaussian is:
$$F(q) = \exp\left(-\frac{1}{2}q^2\sigma^2\right)$$

The convolution theorem is:
$$\Im(f(x) \otimes g(x)) = F(q) \times G(q)$$

Take two Gaussians, $f(x)$ and $g(x)$, with widths σ_1 and σ_2. The Fourier transform of the convolution is:
$$\Im(f(x) \otimes g(x)) = \exp\left(-\frac{1}{2}q^2\sigma_f^2\right) \times \exp\left(-\frac{1}{2}q^2\sigma_g^2\right)$$
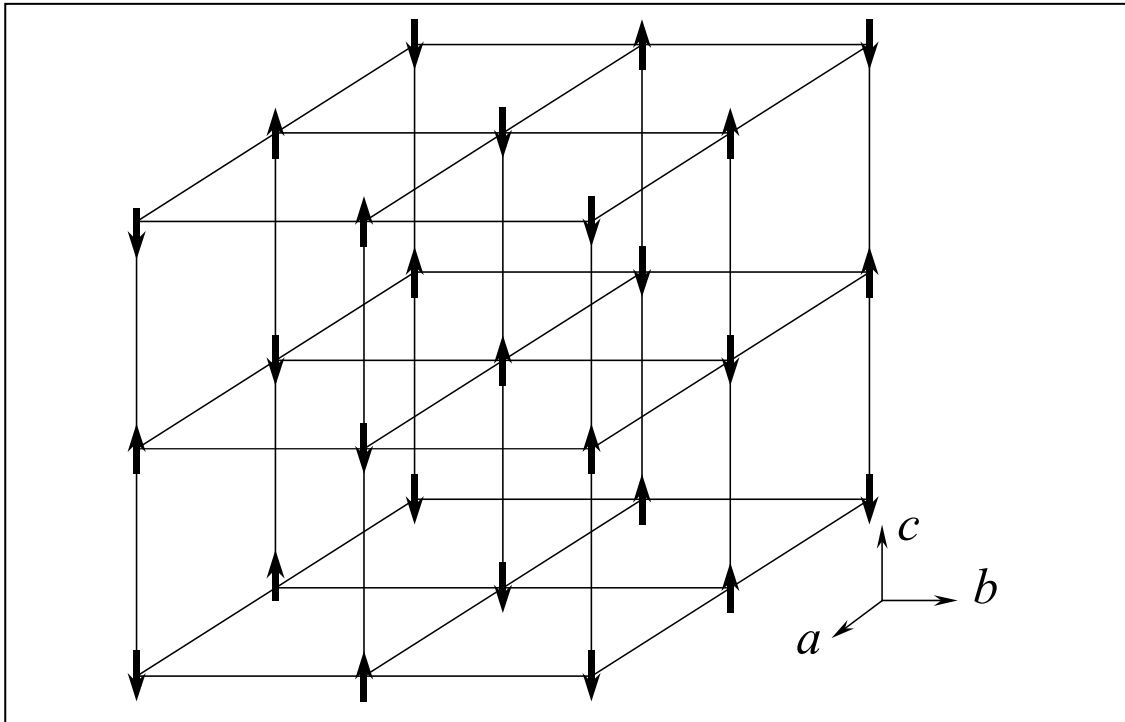$$= \exp\left(-\frac{1}{2}q^2\left(\sigma_f^2 + \sigma_g^2\right)\right)$$

This may now be inverse Fourier transformed to give:
$$f(x) \otimes g(x) = \Im^{-1}\left(\Im(f(x) \otimes g(x))\right)$$
$$= \frac{1}{\sqrt{2\pi\left(\sigma_f^2 + \sigma_g^2\right)}} \exp\left(-\frac{x^2}{2\left(\sigma_f^2 + \sigma_g^2\right)}\right)$$

Hence, the convolution of two Gaussians gives a Gaussian, and its width is given by
$$\sqrt{\sigma_f^2 + \sigma_g^2}$$

D2.1

The moments point along *c* and each atom is antiferromagnetically coupled to its nearest neighbour, i.e. the magnetic unit cell is twice as large along *a*, *b*, and *c*:

D2.2
The nuclear unit cell is primitive, thus Bragg peaks will appear at all the points in *h*, *k* and *l*.

D2.3
The magnetic unit cell is twice as large as the nuclear in *a*, *b* and *c*, hence the magnetic reciprocal lattice is half the size of the nuclear reciprocal lattice.

Nuclear indices written in black, magnetic indices written in red
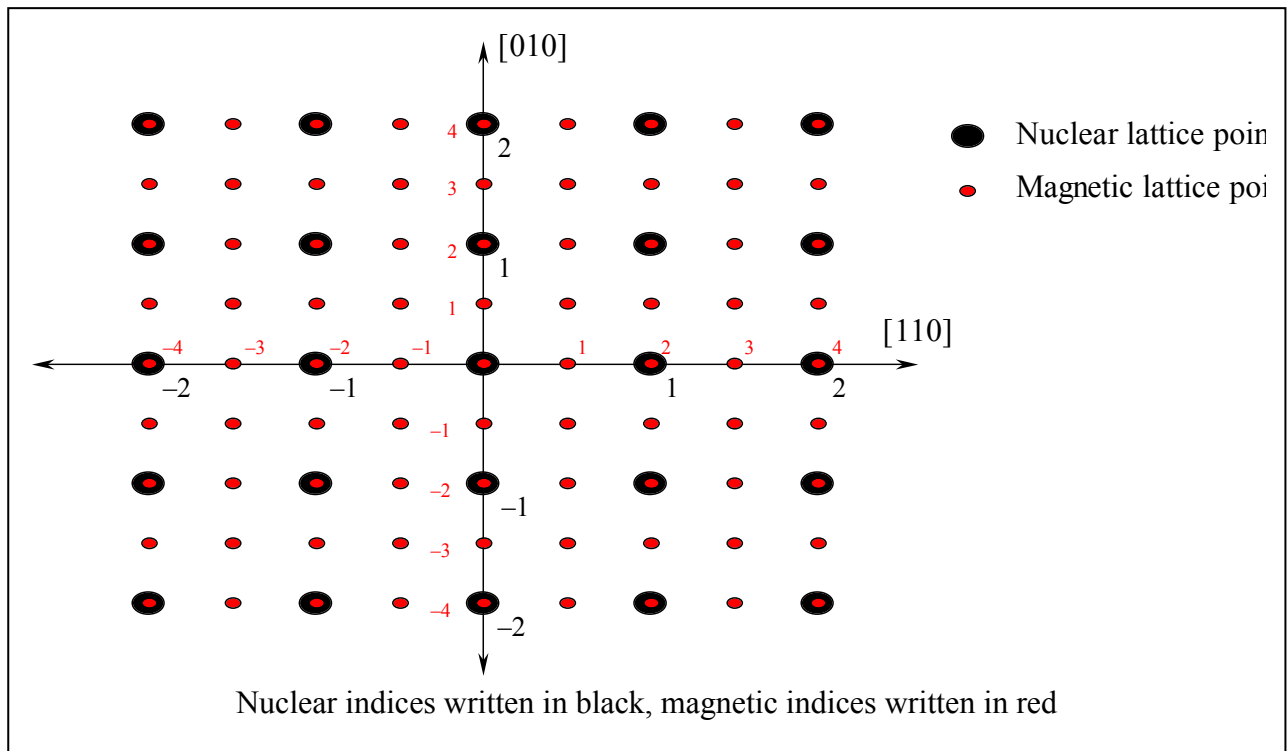
D2.4

The magnetic structure factor is given by the Fourier transform of the moment orientations and positions, i.e.

$$F_{mag}^{hkl} = \sum_{j=1}^{N} \mu_j \exp\left(2\pi i\left(hx_j + ky_j + lz_j\right)\right)$$

where N is the number of moments in the unit cell. There are 8:

Atom	(x,y,z)	Moment amplitude
1	(0, 0, 0)	+1
2	(0.5, 0.5, 0)	+1
3	(0.5, 0, 0.5)	+1
4	(0, 0.5, 0.5)	+1
5	(0.5, 0, 0)	-1
6	(0, 0.5, 0)	-1
7	(0, 0, 0.5)	-1
8	(0.5, 0.5, 0.5)	-1

Note that (x,y,z) are defined with respect to the *magnetic* unit cell, and the amplitude is given in units of μ.

Substitute these values in to the equation, which becomes:

$$F_{mag}^{hkl} = \mu\left(\begin{array}{c} 1 + \exp\left(\pi i(h+k)\right) + \exp\left(\pi i(h+l)\right) + \exp\left(\pi i(k+l)\right) \\ -\exp\left(\pi ih\right) - \exp\left(\pi ik\right) - \exp\left(\pi il\right) - \exp\left(\pi i(h+k+l)\right) \end{array}\right)$$

This equals zero for all *h,k,l* except when they are all odd!

The Bragg peak map therefore looks like:
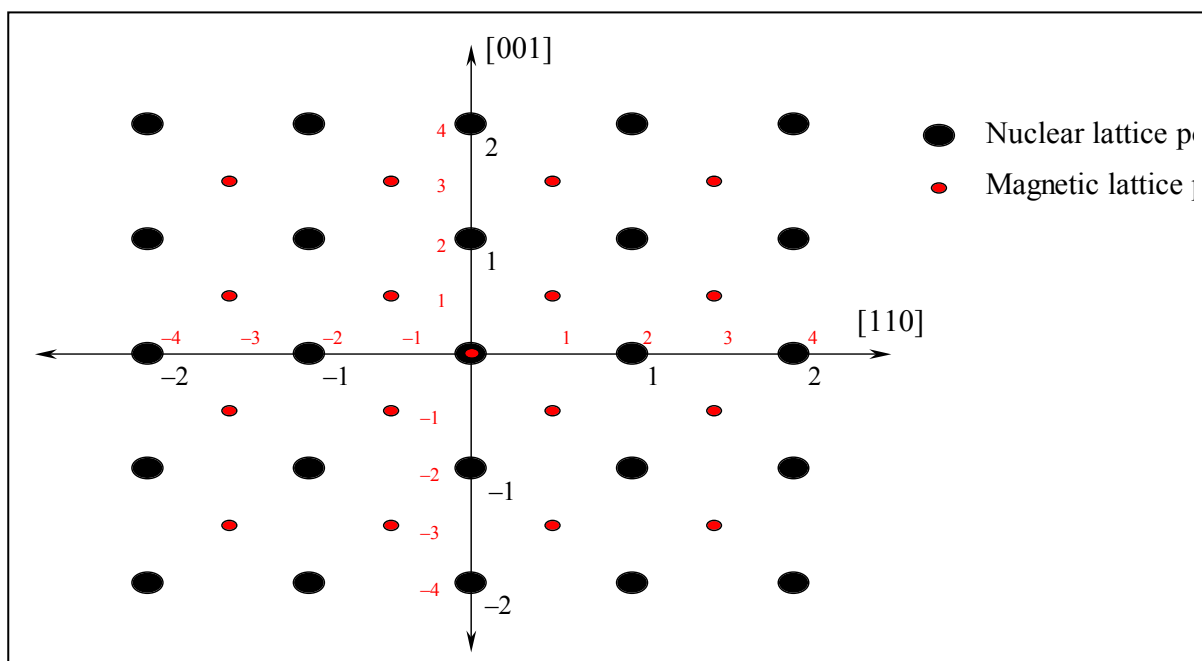
This comes about because the magnetic unit cell has a higher symmetry than the nuclear unit cell. It is, in fact, face-centred cubic with 4 moments in its basis.

The structure factor for all the visible lattice points is 8μ, however the intensities of the Bragg peaks will *not* be all the same (despite them all having the same structure factor). The direction of **Q** with respect to the moment direction becomes important. Neutrons only ever see the perpendicular component of the sublattice magnetization to **Q**, thus the intensity of the Bragg peaks will be multiplied by $\sin^2\phi$, where ϕ is the angle between **Q** and [001]. Furthermore, the intensity will be modulated by the magnetic form factor. This will cause the intensity to *decrease* with *increasing Q*.

D2.5 The spin waves will be visible in both directions. However, the spin waves in the classical picture take the form of fluctuations that are perpendicular to the mean moment direction. Hence, if the moments are oriented along *c*, the spin waves will take the form of fluctuations in the (*a, b*) plane. Measurements along the [001] axis will therefore see the full contribution from the spin waves as this direction is normal to the (*a, b*) plane, as **Q** is always perpendicular to the moment contributions. Measurements along the [110] axis will only have half this intensity as components of the spin waves along [110] will not give any neutron scattering.

D2.6 If the sample has many domains, there will be no distinction between moments lying along *a*, *b*, or *c*. Therefore the $\sin^2\phi$ term will need to be averaged over all possible orientations, i.e. the magnetic (511) and (333) peaks (which have the same *Q*) will have the same intensity.

E. Incoherent Inelastic Scattering
(with a Pulsed Neutron Spectrometer)

E1.

(i) The elastic peak in Figure E.2 occurs at the t.o.f.:

$$t \approx 64.1 ms \quad .$$

The total flight path is 36.54m +1.47m=38.01m , and so the neutron velocity is

$$v_n = 0.593 \, kms^{-1}$$

and the energy selected by the crystal analyser is

$$E_n = \tfrac{1}{2} m_n v_n^2 = \underline{\textbf{1.85 meV}} \, .$$

(ii) The Bragg angle θ_A of the analyser is given by

$$\theta_A = \arcsin\left(\frac{\lambda}{2 d_{002}}\right) \, ,$$

where $\lambda = \dfrac{h}{m_n v_n} = 6.67\text{Å}$. Thus $\underline{\theta_A \approx \textbf{85}^\circ}$.

(iii) The advantage of using a high take-off angle $\left(170^\circ\right)$ is that the wavelength band reflected by the analyser is then relatively small.

E2.

For neutron-energy gain the flight-time is greater than it is for elastic scattering, whereas for neutron-energy loss the flight-time is less than for elastic scattering. Thus the inelastic peaks in Figure E.2 are at $t \approx 65.7ms$ for energy gain and at $t \approx 62.7ms$ for energy loss.

The sample-analyser-detector distance is 1.47m and the total flight-path is 38.01m. The elastically-scattered neutrons cover the total flight path in 64.1ms, and so they cover the sample-analyser-detector distance in $64.1 \times (1.47/38.01)ms = 2.48ms$. The moderator-to-sample distance of 36.54m is covered by the energy-gain neutrons in the time

$$(65.7\text{-}2.48)ms = 63.2ms.$$

Hence the energy of these neutrons is

$$E_{gain} = \frac{1}{2}m_n v_n^2 = \frac{1}{2}m_n \left(\frac{36.54m}{63.2ms}\right)^2$$

or
$$E_{gain} = \underline{\mathbf{1.76meV}} .$$

A similar calculation for the energy-loss neutrons gives

$$E_{loss} = \underline{\mathbf{1.94meV}} .$$

We see, therefore, that the energy transfer is $\underline{\pm\mathbf{0.09}meV}$.

E3

(i) The intensity is influenced by the Bose factor $n(E)$ which gives the number of phonons which exist at a given energy E and temperature T :

$$n(E) = \frac{1}{\exp\left(\dfrac{E}{k_B T}\right) - 1} \ .$$

For neutron-energy loss the intensity is proportional to $[1 + n(E)]$, whereas for neutron-energy gain it is proportional to $n(E)$. At low temperatures $n(E)$ tends to zero and only scattering with neutron energy loss ('down scattering') is possible. There is always a greater possibility, at any temperature, that neutrons will be scattered with energy loss.

F. Coherent Inelastic Scattering
(with a Three-Axis Spectrometer)

F1.

The allowed points have *hkl* indices, which are all odd or all even. See Figure F1a.

F2.

The relation between neutron energy E and neutron wave number k is

$$E(meV) = 2.072\left[k(\mathring{A}^{-1})\right]^2 \ .$$

Putting $E_i^{min} = 3meV$ and $E_i^{max} = 14meV$ gives

$$k_i^{min} = \underline{\textbf{1.203}\ \mathring{A}^{-1}} \text{ and } k_i^{max} = \underline{\textbf{2.600}\ \mathring{A}^{-1}}..$$

We also have $k = 2\pi/\lambda$, so that k_i^{min} corresponds to the maximum wavelength $\lambda_i^{max} = \underline{\textbf{5.22}\ \mathring{A}}$, and k_i^{max} to the minimum wavelength $\lambda_i^{min} = \underline{\textbf{2.42}\ \mathring{A}}$.

F3

(i) We have $Q_{220} = 2\pi/d_{220} = \sqrt{8}\left(2\pi/a_0\right)$, so that $Q_{220} = \underline{\textbf{3.20}\ \mathring{A}}$.

Figure F1a shows the vectors $\mathbf{k}_i$, $\mathbf{k}_f$, and $\mathbf{Q}$ for the *220* reflection.

(ii) Putting $k_i = k_f$ into $Q^2 = k_i^2 + k_f^2 - 2k_ik_f\cos\phi$ we get
$$\phi = 2\sin^{-1}(Q/2k_i),$$

and so $\phi = \underline{\textbf{75.9}\ °}$.

(iii) In the case of elastic scattering the scattering angle ϕ is twice the Bragg angle θ_B.
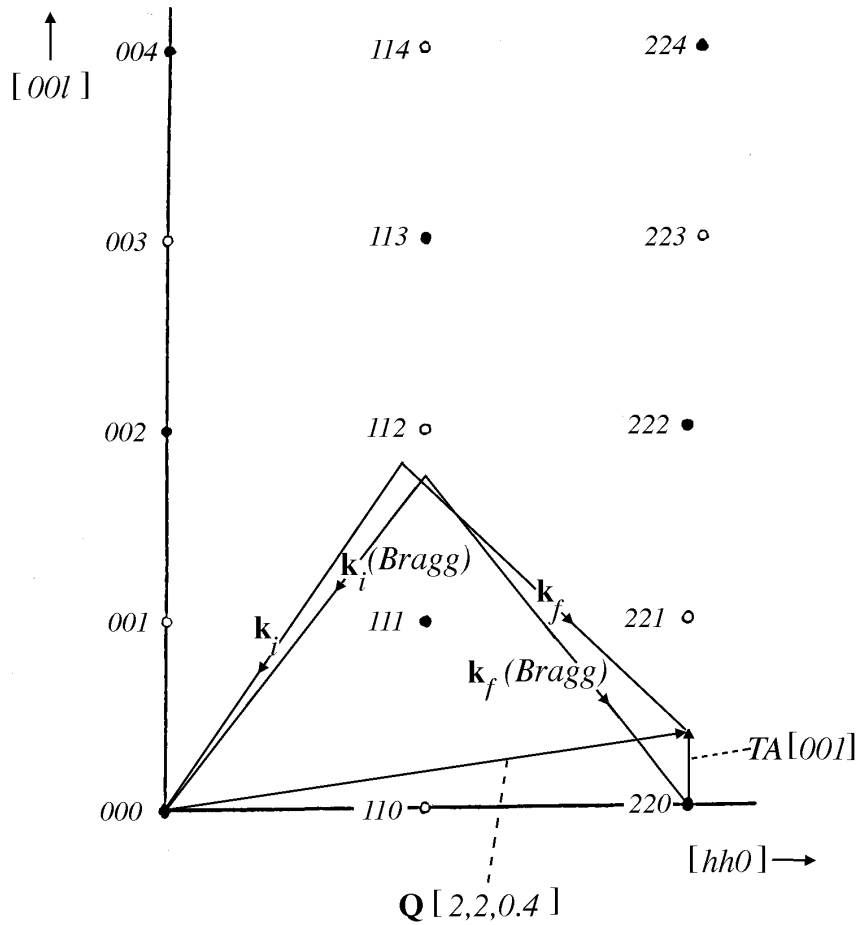
F4.

See Figure F1a.

Figure F.1a. *Reciprocal lattice construction for 220 Bragg scattering and for inelastic scattering by the transverse acoustic [001] phonon.*

F5.

The vector $\mathbf{Q}[2, 2, 0.4]$ (Figure F1a) is of magnitude

$$Q = 2\pi/a_0 \cdot \sqrt{4 + 4 + 0.16} = 3.228 \AA^{-1}.$$

We have $E_i^{max} = 14 meV$ and $\Delta E = 3 meV$. Hence for neutron energy loss $E_f = 11 meV$ and for neutron energy gain $E_f = 17 meV$. Using eqn. (F4) we get $k_f = 2.304 \AA^{-1}$ for energy loss and $k_f = 2.864 \AA^{-1}$ for energy gain. From eqn. (F2) we then have $\phi = 82.1°$ (loss) and $\phi = 72.2°$ (gain)

.

F6.

The resolution is best for small k_f, i.e. for energy loss. In Figure F.1* the vectors $\mathbf{k}_i$ and $\mathbf{k}_f$ are drawn for this configuration.

F7.

(i) At 300K: $n(E)$=8.3 for energy gain and $n(E) + 1 = 9.3$ for energy loss. At 0K: $n(E)$=0 for energy gain and $n(E) + 1 = 1$ for energy loss.

(ii) Thus it doesn't make much difference at 300K whether one works in energy gain or in energy loss, but at low temperatures one must work in energy loss.

F8.

No; not with this value of the incident wavelength. We have $Q_{440} = 2Q_{220}$ $= 6.46 Å^{-1}$, $k_i + k_f = 4.904 Å^{-1}$ in energy loss , and $k_i + k_f = 5.464 Å^{-1}$ in energy gain. Hence $k_i + k_f < Q$ and it is impossible to close the scattering triangle (Figure F.2) in either case.

G. Disordered Materials Diffraction

G1.1 a) and c)

Lennard-Jones potential
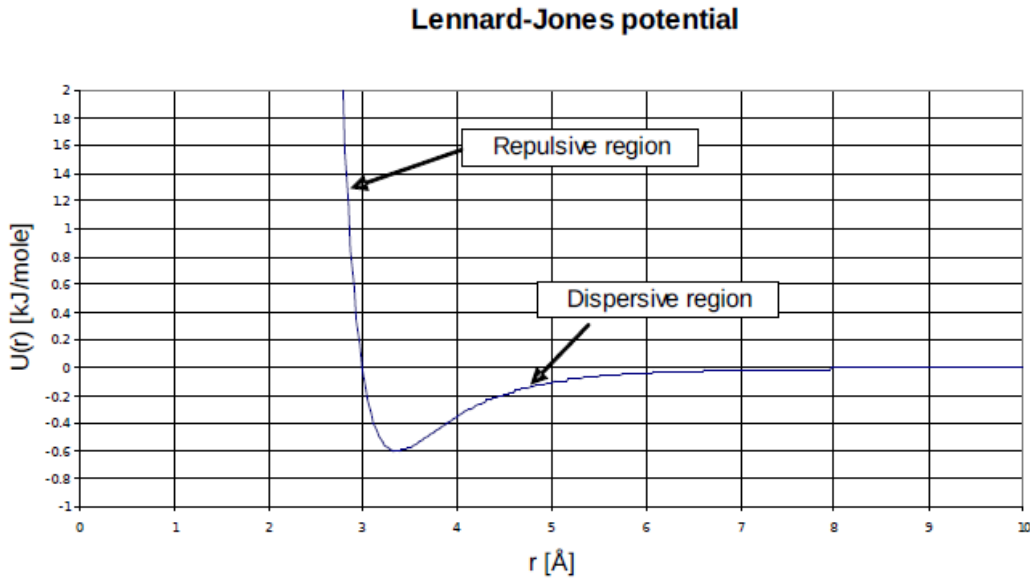
G1.1 b)

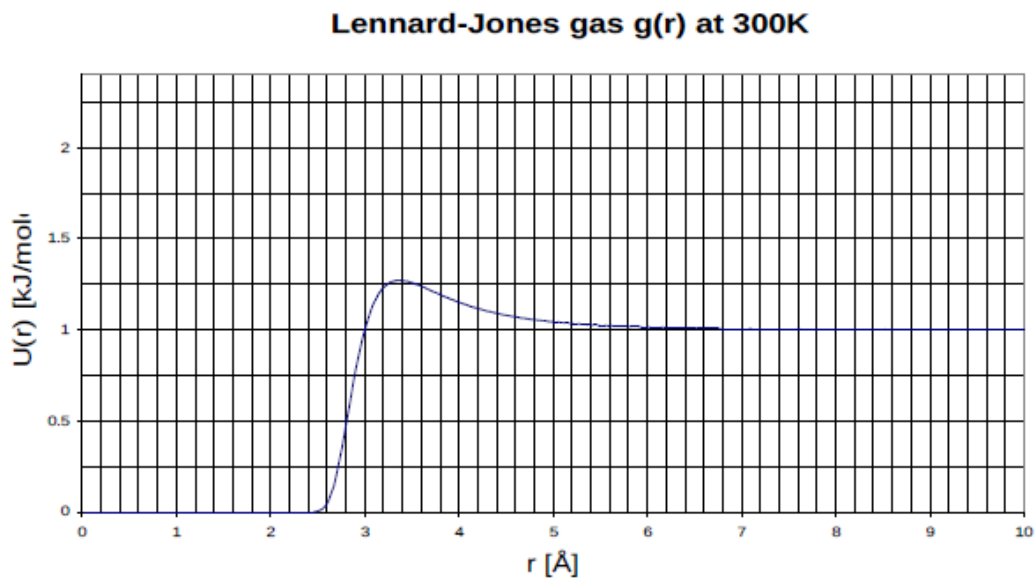ε represents the depth of the potential. It controls how tightly adjacent atoms are bound. σ represents the radius at which the hard core repulsive region goes to zero. It represents roughly the distance of closest approach of two atoms.

G1.2 a)

Lennard-Jones gas g(r) at 300K

G1.2b)

At low *r*, *U(r)* becomes very large, while *g(r)* goes to zero. At high *r*, *U(r)* goes to zero, while *g(r)* goes to unity. In between the two functions are in rough antiphase.

G1.2c) If ε were increased by a factor of 2, the height of the peak in *g(r)* at ~ 3.8Å would grow from ~1.27 to ~1.54. If σ were increased by 20%, the main peak would move out by 20%, but would remain the same height.

G1.3a)
In the gas form *g(r)* decays monotonically to unity at large r. As the density increases the height of the main peak increases and it becomes sharper as a series of decaying oscillations occur towards larger r. All the peaks move to smaller r with increasing density.

Based on a change of density of 0.02 to 0.035, one might expect the separation of peaks to change by the cube root of the ratio of densities, namely

$$\sqrt[3]{0.02/0.035} = 0.83$$

In fact the first peak moves from 3.18Å to 3.06Å, a fractional change of only 0.96, while the second peak moves from 6.39Å to 5.91Å, a fractional change of 0.92. In other words the peaks in *g(r)* do NOT represent the mean separation of the atoms. This can be quite confusing!

G1.3b)
Fundamentally as the material becomes more dense the direct interactions between atoms 1 and 2 become increasingly affected by the presence of 3rd, 4th , etc. atoms which increasingly surround them, and which increasingly confine them in space. Within the pairwise additive approximation assumed here all the atoms interact via known pairwise forces, but the result is many body correlations which are difficult to predict accurately. A raft of theoretical methods to do this approximately exist, but few if any of them work for the kind of interatomic forces that are found in real materials. Hence in practice one has little option but to use computer simulation to determine the effect of many-body correlations in real materials. This problem affects crystals as much as it affects liquids, but in a crystal one has a repeat lattice (which is itself a consequence of many body correlations) which we can determine from the position and height of the Bragg peaks. In any case the primary goal of interest in crystallography is the single particle correlation function (the lattice), not the higher order correlations. The single particle correlation function for a liquid is uniform and contains no information. For a glass it is not uniform, but contains no repeat distances.

G1.4a)

For density 0.02 the first minimum occurs at 4.95Å, giving a coordination number of ~10 atoms. For density 0.035, the first minimum is at 4.47 Å with a coordination number of 12.5. Clearly these numbers do not scale with density change: coordination number varies less rapidly than the density.

G1.4b)

If instead we had used the same radius, 4.47 Å, then the coordination number at density 0.02 is 7.23, a ratio of 0.58 compared to density 0.035, which is quite close to the ratio of densities, 0.57. This illustrates again that peaks and dips in g(r) do not correlate directly with the density, although they are obviously related to it.

G1.5a)

The primary effect of changing the density on the structure factor is to increase the amplitude of the oscillations. There is some movement of the peaks as well, but fundamentally as the density increases they become sharper, and the oscillations extend to large Q.

G1.5b)

For density 0.02, the first peak in *g(r)* is at 3.18Å and the first peak in S(Q) is at 2.2Å-1. For density 0.035, the first peak in *g(r)* is at 3.06Å and the first peak in S(Q) is at 2.35Å^{-1}, i.e. as the peaks in *g(r)* move in, those in *S(Q)* move out, although the movement of the first peak in *S(Q)* is more related to the movement of the 2nd and subsequent peaks in *g(r)* than it is to the first peak in *g(r)*.

G1.5c)

It depends how we did it. If we increased σ at constant density, then the peaks would move out, but also become markedly sharper as the packing fraction of the liquid increased. If the density was reduced to compensate for the increase (atoms occupying more space) then the peaks in *S(Q)* would move in, but without increased amplitude.

G1.5d)

Since the structure factor only exists if the density is finite, a zero density will produce zero structure factor.

G2.1a)

Atomic fractions are $c_{Zn} = 1/3 = 0.333$, $c_{Cl} = 2/3 = 0.667$

G2.1b)

$$F(Q) = \frac{1}{9} b_{Zn}^2 H_{ZnZn}(Q) + \frac{4}{9} b_{Zn} b_{Cl} H_{ZnCl}(Q) + \frac{4}{9} b_{Cl}^2 H_{ClCl}(Q)$$

G2.1c)

In essence the idea is that we measure *F(Q)* for three samples, namely one with only ^{35}Cl isotope present, another with only ^{37}Cl isotope present, and a third with a mixture of x parts ^{35}Cl and (1-x) parts of ^{37}Cl. For this third sample the chlorine scattering length is

$$b_{mix} = x b_{35_{Cl}} + (1-x) b_{37_{Cl}}$$

which means the weighting coefficient of the H_{ClCl} partial structure factor for this sample is not a linear combination of the same coefficient for the other two samples. This means the determinant of coefficients in the above formula for the three samples is finite and the matrix of coefficients can be inverted. Hence the three measurements can be used to extract the three partial structure factors, at least in principle.

A basic assumption of the isotope substitution method is that the partial structure factors do not change appreciably with isotopic composition of the sample. This is an accurate assumption in most cases, but is less accurate when hydrogen is replaced with deuterium, particularly at low temperatures and with larger molecules, because in these cases quantum effects due to the different masses can impact on both the structure and the phase diagram of the material in question.

G2.1d)

Remarkably few in practice. There have been attempts to perform isomorphic substitution with X-rays, but these method tends to be shrouded in uncertainties from knowing whether one atom can substitute for another without . Then there has been the combination of neutrons, X-rays and electrons, but each technique requires quite different sample containment, making comparisons of the three results dubious. A more promising approach is the use of anomalous dispersion of Xrays, whereby you vary the scattering length of one component near an absorption edge. This method is quite promising, but requires highly stable precision equipment to be performed satisfactorily, and to date has only be tried on a handful of materials. It suffers also from poor counting statistics because of the high degree of monochromatisation needed for the incident beam of X-rays. Recently we have been exploring the use EXAFS to refine liquid and glass structures, and this approach looks very promising indeed.

G2.2a)

This is a very common problem in neutron scattering using isotopes: one or more of the components makes only a small contribution to the scattering pattern. In this case it is the ZnZn structure factor. Below is shown the inversion of the weights matrix:-

Partial Structure Factor	$Zn^{35}Cl_2$	$Zn^{mix}Cl_2$	$Zn^{37}Cl_2$
Zn-Zn	37.25	-71.53	62.16
Zn-Cl	-21.87	39.37	-17.50
Cl-Cl	10.15	-14.99	4.84

Table II: Inversion of the matrix coefficients of Table I

You will notice that to extract the ZnZn partial structure factor we need to multiply the data by large numbers and then add and subtract them, making us rely heavily on the absolute accuracy of the diffraction data if we are to avoid amplifying systematic data errors in the final structure factor. Obtaining absolute scattering cross sections with accuracies better than 1% is a tall order with any technique, including neutrons, and is rarely achieved.

G2.2b)
Particular difficulties are:-

a) The data are only available over a finite Q range;

b) The data are multiplied by Q in the integrand of (1.5) making the effect of statistical uncertainty at high Q a particular difficulty.

c) No matter how careful they are measured and corrected, diffraction data always have systematic errors, which can seriously perturb the Fourier transform, particularly at low r.

Fourier transform of data with potential significant systematic error is risky: the systematic error can have the effect of introducing marked backgrounds in real space that can make the peaks larger or smaller than they should be. As a consequence coordination numbers can be faulty when extracted by this method.

G2.2c)
Fourier transforms of raw data should be avoided whenever possible. Instead the data should be compared with a structural model of the data, and then, assuming the model is satisfactory, use the model to generate the real space distributions, as well as address other questions about the structure of the material. Computer simulation is a convenient method to produce such a structural model of the measured scattering cross sections. This model will also help to identify what might be wrong (if there is anything) with the data, and avoid some of the problems introduced by systematic effects. Some authorities

are reluctant to use computer simulation to achieve this, since it too can introduce systematic bias in the interpretation of the data, and so instead invoke a series of consistency checks on the data. These are used to identify and correct particular problems with the data, but this can be a very time consuming process which can take months to resolve. The net effect is the same however: in computer simulation one is already applying a series of physical consistency checks on the data, with the advantage that you have at the end a physical model of the scattering system which is consistent with your scattering data. With the other methods, you have corrected data, but you still have the problem of trying to understand what they mean.

G2.3a)
Figure G2.2 shows the running coordination number of this *g(r)*. From this graph we can read that at the first minimum, 3.4Å, the running coordiation number is ~4.3 Cl about Zn. Since there are half the number Zn atoms compared to Cl, the coordination number of Zn about Cl will be 2.2.

G2.3b)
The first ZnCl peak is at 2.31Å, while the first ClCl distance is at 3.69Å. Using the cosine rule, I estimate the Cl-Zn-Cl angle to be 106º, which is close to the tetrahedral angle of 109.47º. This together with the coordination number of ~4 is a strong hint of likely tetrahedral local coordination in this liquid.

Taking this argument a bit further, one notices that the first ZnZn peak is at 3.93Å, while the second is at 6.81Å, giving a Zn-Zn-Zn angle of 120º, suggesting also that at least the Zn packing is not simple, and probably maps into the roughly tetrahedral packing of the Cl around Zn, with significant edge-sharing of the tetrahedra.

G2.3c)
Looking at the curves one is struck by the way the ZnCl oscillations are almost exactly out of phase with the ZnZn and ClCl oscillations. This behaviour strongly indicative of charge ordering, although it is not entirely clear that Zn and Cl are fully ionic in this system.

H: Polarized Neutrons

H1. a) Flipping ratio: $F = N_+ / N_- = 51402 / 1903 = \underline{27 \;+/-\; 0.6}$

$$\{error\; bar\; dF = \sqrt{\left(\frac{dN_+}{N_-}\right)^2 + \left(\frac{dN_- N_+}{N_-^2}\right)^2} \;=> dF = 0.63\}$$

Therefore, the polarization is: $P = F - 1 / F + 1 = \underline{0.929 \;+/-\; 0.002}$

$$\{error\; bar\; dP = \left(\frac{2}{(F+1)^2}\right) dF \;=> dF = 0.002\;\}$$

b) Systematic errors in this measurement will largely arise from background contributions from the instrumental environment. In order to measure a reliable flipping ratio, the N_+ and N_- counts must be measured with and without the sample in the beam. The flipping ratio is then given by

$$F = \frac{N_+^{sample} - N_+^{empty}}{N_-^{sample} - N_-^{empty}}$$

Other sources of systematic error will be different values of the polarizing power of the polarizer and analyser, in addition to the finite flipping efficiency of the flipper.

H2. a)   The adiabacity parameter is given by $E = \dfrac{\omega_L}{\omega_B}$

The Larmor frequency, $\omega_L = \gamma B$, where the gyromagnetic ratio, γ is given by the ratio of the neutron magnetic moment to its angular momentum ($= \frac{1}{2}\hbar$)

Therefore: $\omega_L = \dfrac{2\mu_n B}{\hbar} = 1.83\times10^8 B$ rad s^{-1} with B given in T.

In this example, B = 3 mT and is constant in magnitude, $=> \omega_L = 5.49 \times 10^5$ rad s^{-1}

Now: $\omega_B = \dfrac{d\theta}{dy} v = \dfrac{\pi/2}{0.1} v = 15.71 v$

Expressing v in terms of λ: $E = \dfrac{h^2}{2m_n\lambda^2} = \dfrac{m_n v^2}{2} \Rightarrow v = \dfrac{h}{m_n\lambda} = \dfrac{3956}{\lambda}$ with v in m s^{-1} and λ in Å.

So: $\omega_B = 15.71\frac{3956}{2} = 31074\,\text{rad s}^{-1}$.

The adiabacity parameter is therefore: $\underline{E = 17.7}$ and the field/flipper design should successfully propagate the neutron polarization and flip the spins without significant depolarization.

b) The design could be improved by either increasing the guide fields (and the current in the Dabbs foil) or by lengthening the distance over which the field rotates by 90°.

H3. a) The number of neutrons transmitted through an absorbing material is: $n = n_0\exp(-N\sigma t)$ where n_0 is the initial number of neutrons, N is the number density of atoms in the material, σ is the mean absorption cross-section and t is the thickness of the material. So the numbers of $+$ and $-$ neutrons transmitted is:

$$n_+ = n_0\exp(-N\sigma_+ t) = n_0\exp(-N\sigma_0 t)\exp(-N\sigma_p t)$$

$$n_- = n_0\exp(-N\sigma_- t) = n_0\exp(-N\sigma_0 t)\exp(N\sigma_p t)$$

Therefore the polarization is:

$$P = \frac{n_+ - n_-}{n_+ + n_-} = \frac{\exp(-N\sigma_p t) - \exp(N\sigma_p t)}{\exp(-N\sigma_p t) + \exp(N\sigma_p t)} = -\tanh(N\sigma_p t)$$

The transmission of each spin state is: $T_\pm = \dfrac{n_\pm}{n_0} = \exp(N\sigma_\pm t)$

Therefore the total transmission:

$$T = \frac{T_+ + T_-}{2} = \exp(-N\sigma_0 t)\frac{\exp(-N\sigma_p t) + \exp(N\sigma_p t)}{2} = \exp(-N\sigma_0 t)\cosh(N\sigma_p t)$$

b) The expression for the spin-dependent absorption of a nuclear spin filter is

$\sigma_\pm = \sigma_a(E)(1 \pm \rho P_N)$ where, P_N is the nuclear polarization and $\sigma_a(E)$ is the energy dependent absorption cross-section. The constant ρ is given by the expressions:

$$\rho = \frac{I(1-2x) - x}{I+1}, \quad \text{where } x = \frac{\sigma_{I-1/2}}{\sigma_{I+1/2} + \sigma_{I-1/2}}.$$

Since ^{3}He absorbs only through the $I - \frac{1}{2}$ channel, we may put $\sigma_{I+1/2} = 0$, and therefore:

$\rho = -1$.

Therefore: $\sigma_\pm = \sigma_a(E)(1 \mp P_{He}) = \sigma_0 \pm \sigma_p$

So, equating the spin-independent and spin-dependent parts of the expression, we get

$$\sigma_0 = \sigma_a(E)$$

$$\sigma_p = -\sigma_0 P_{He} \Rightarrow P_{He} = -\frac{\sigma_p}{\sigma_0}$$

Substituting this back into the general expressions for the spin-filter polarization and transmission, we get:

$P = \tanh(P_{He}N\sigma_0 t)$ and $T = \exp(-N\sigma_0 t)\cosh(P_{He}N\sigma_0 t)$

H4. The expression for the differential cross-section from a magnetised crystal, with magnetisation direction $\hat{\eta}$ perpendicular to the scattering vector **Q**, we have

$$\frac{d\sigma}{d\Omega} = F_N^2(\mathbf{Q}) + 2F_N(\mathbf{Q})F_M(\mathbf{Q})[\mathbf{P}\cdot-\hat{\eta}] + F_N^2(\mathbf{Q})$$

Therefore the expressions for n_+ ($\mathbf{P}\cdot-\hat{\eta}=-1$) and n_- ($\mathbf{P}\cdot-\hat{\eta}=1$) are

$$n_+ = (F_N - F_M)^2$$

$$n_- = (F_N + F_M)^2$$

Therefore, the polarization is:

$$P = \frac{(F_N - F_M)^2 - (F_N + F_M)^2}{(F_N - F_M)^2 + (F_N + F_M)^2} = \frac{-4F_N F_M}{2F_N^2 + 2F_M^2} = \frac{-2F_N F_M}{F_N^2 + F_M^2}$$

The minus sign indicates that the neutrons are polarized antiparallel to the direction of magnetisation of the crystal.

H5. The first rule of thumb in magnetic polarized neutron scattering is that spin-flipped neutrons will only be produced by components of the sample magnetisation perpendicular to the neutron polarization direction. [This is an extremely useful rule to bear in mind during all polarized neutron experiments.] Therefore, if we are scattering neutrons from a fully magnetised scatterer (i.e. a ferromagnet for example) – magnetised in the direction of the neutron polarization (which is an experiment necessity), then there will be no perpendicular components of the magnetisation, and therefore no spin-flip scattering. We can therefore dispense with the analysers, since the scattered beam remains fully polarized.

H6. a) The Pauli spin relations are:

$$\sigma_x|\uparrow\rangle = \begin{vmatrix} 0 & 1 \\ 1 & 0 \end{vmatrix}\begin{vmatrix} 1 \\ 0 \end{vmatrix} = \begin{vmatrix} 0 \\ 1 \end{vmatrix} = |\downarrow\rangle$$

$$\sigma_x|\downarrow\rangle = \begin{bmatrix} 0 & 1 \\ 1 & 0 \end{bmatrix}\begin{bmatrix} 0 \\ 1 \end{bmatrix} = \begin{bmatrix} 1 \\ 0 \end{bmatrix} = |\uparrow\rangle$$

$$\sigma_y|\uparrow\rangle = \begin{bmatrix} 0 & -i \\ i & 0 \end{bmatrix}\begin{bmatrix} 1 \\ 0 \end{bmatrix} = i\begin{bmatrix} 0 \\ 1 \end{bmatrix} = i|\downarrow\rangle$$

$$\sigma_x|\downarrow\rangle = \begin{bmatrix} 0 & -i \\ i & 0 \end{bmatrix}\begin{bmatrix} 0 \\ 1 \end{bmatrix} = -i\begin{bmatrix} 1 \\ 0 \end{bmatrix} = -i|\uparrow\rangle$$

$$\sigma_z|\uparrow\rangle = \begin{bmatrix} 1 & 0 \\ 0 & -1 \end{bmatrix}\begin{bmatrix} 1 \\ 0 \end{bmatrix} = \begin{bmatrix} 1 \\ 0 \end{bmatrix} = |\uparrow\rangle$$

$$\sigma_z|\downarrow\rangle = \begin{bmatrix} 1 & 0 \\ 0 & -1 \end{bmatrix}\begin{bmatrix} 0 \\ 1 \end{bmatrix} = -\begin{bmatrix} 0 \\ 1 \end{bmatrix} = -|\downarrow\rangle$$

b) Now, we have to calculate the matrix element for magnetic scattering $\langle S'|V_m|S\rangle$, where S' and S are the final and initial spin states, and V_m is the magnetic interation potential, which is given by

$$V_m = \frac{-\gamma_n r_0}{2m_n}\sum_\zeta \sigma_\zeta M_{\perp\zeta}$$

Therefore, the 4 possible spin-transitions are given by
i) Non-spin-flip: $|\uparrow\rangle \rightarrow |\uparrow\rangle$

$$\langle\uparrow|V_m|\uparrow\rangle = \frac{-\gamma_n r_0}{2m_n}\left(\langle\uparrow|\sigma_x|\uparrow\rangle M_{\perp x} + \langle\uparrow|\sigma_y|\uparrow\rangle M_{\perp y} + \langle\uparrow|\sigma_z|\uparrow\rangle M_{\perp z}\right)$$

$$= \frac{-\gamma_n r_0}{2m_n}\left(\langle\uparrow|\downarrow\rangle M_{\perp x} + i\langle\uparrow|\downarrow\rangle M_{\perp y} + \langle\uparrow|\uparrow\rangle M_{\perp z}\right)$$

$$= \frac{-\gamma_n r_0}{2m_n}M_{\perp z}$$

ii) Non-spin-flip: $|\downarrow\rangle \rightarrow |\downarrow\rangle$

$$\langle\downarrow|V_m|\downarrow\rangle = \frac{-\gamma_n r_0}{2m_n}\left(\langle\downarrow|\sigma_x|\downarrow\rangle M_{\perp x} + \langle\downarrow|\sigma_y|\downarrow\rangle M_{\perp y} + \langle\downarrow|\sigma_z|\downarrow\rangle M_{\perp z}\right)$$

$$= \frac{-\gamma_n r_0}{2m_n}\left(\langle\downarrow|\uparrow\rangle M_{\perp x} - i\langle\downarrow|\uparrow\rangle M_{\perp y} - \langle\downarrow|\downarrow\rangle M_{\perp z}\right)$$

$$= \frac{-\gamma_n r_0}{2m_n}\left(-M_{\perp z}\right)$$

iii) Spin-flip: $|\!\uparrow\rangle \rightarrow |\!\downarrow\rangle$

$$\langle\uparrow|V_m|\downarrow\rangle = \frac{-\gamma_n r_0}{2m_n}\left(\langle\uparrow|\sigma_x|\downarrow\rangle M_{\perp x} + \langle\uparrow|\sigma_y|\downarrow\rangle M_{\perp y} + \langle\uparrow|\sigma_z|\downarrow\rangle M_{\perp z}\right)$$

$$= \frac{-\gamma_n r_0}{2m_n}\left(\langle\uparrow|\uparrow\rangle M_{\perp x} - i\langle\uparrow|\uparrow\rangle M_{\perp y} - \langle\uparrow|\downarrow\rangle M_{\perp z}\right)$$

$$= \frac{-\gamma_n r_0}{2m_n}\left(M_{\perp x} - iM_{\perp y}\right)$$

iv) Spin-flip: $|\!\downarrow\rangle \rightarrow |\!\uparrow\rangle$

$$\langle\downarrow|V_m|\uparrow\rangle = \frac{-\gamma_n r_0}{2m_n}\left(\langle\downarrow|\sigma_x|\uparrow\rangle M_{\perp x} + \langle\downarrow|\sigma_y|\uparrow\rangle M_{\perp y} + \langle\downarrow|\sigma_z|\uparrow\rangle M_{\perp z}\right)$$

$$= \frac{-\gamma_n r_0}{2m_n}\left(\langle\downarrow|\downarrow\rangle M_{\perp x} + i\langle\downarrow|\downarrow\rangle M_{\perp y} + \langle\downarrow|\uparrow\rangle M_{\perp z}\right)$$

$$= \frac{-\gamma_n r_0}{2m_n}\left(M_{\perp x} + iM_{\perp y}\right)$$

These equations show that the magnetic non-spin-flip scattering is entirely due to the component of the magnetisation parallel to the neutron polarization direction, $M_{\perp z}$; and that the magnetic spin-flip scattering is entirely due to the components of the magnetisation perpendicular to the neutron polarization direction, $M_{\perp x}$ and $M_{\perp y}$.

H7. From the previous question (which is a derivation of the magnetic part of the Moon, Riste and Koehler equations) we have established that spin-flip scattering arises solely from the components of the sample magnetisation perpendicular to the neutron polarization.
Now, the definition of the neutron sensitive sample magnetisation is
$M_\perp(\mathbf{Q}) = -2\mu_B\left[\boldsymbol{\eta} - (\boldsymbol{\eta}\cdot\hat{\mathbf{Q}})\hat{\mathbf{Q}}\right]$ where $\boldsymbol{\eta}$ is the sample magnetisation (see, for example, Squires, or previous lectures on magnetic scattering).
From this equation, we note that if the scattering vector is parallel to the sample magnetisation, then the neutron sensitive magnetisation is zero.

Therefore, if the neutron polarization is parallel to the scattering vector, the only components of the magnetisation that will scatter neutrons will be perpendicular to the polarization, and will therefore flip the neutron spins.

H8. The advantage of the X-Y-Z difference method of magnetic scattering separation over the method of measuring with the neutron polarization **P** ‖ **Q**, is that the X-Y-Z method applies to a general multi-detector instrument. The **P** ‖ **Q** method only works for one scattering vector at a time.

A further advantage of X-Y-Z is that it is insensitive to background, since the spin-flip background will be the same in Z, X and Y directions, and will therefore cancel out.

I. High resolution spectroscopy
(TOF, backscattering and Spin-Echo)

The aim of this section is to get a feeling for the energy resolution of different spectrometer types: time-of-flight (TOF), backscattering (BS) and spin echo (NSE) spectrometers.

All the following calculations assume a **neutron wavelength of λ=6.3 Å**.

Planck's constant is h=6.6225 10^{-34} Js, sometimes usefully expressed as h = 4.136 µeV ns. Neutron mass m_n=1.675 10^{-27} kg.

I1.

Calculate the neutron speed v_n in [m/s] and the neutron energy in µeV.
v_n=___630___ m/s; En= ___2080___µeV.
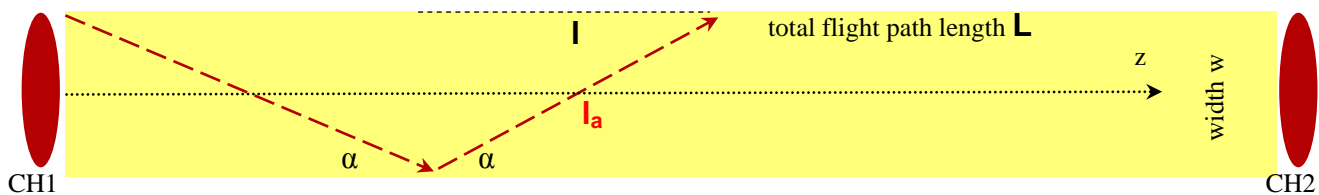
I2. - Time-of-flight spectroscopy

Figure I1. *Time-of-flight spectrometer with two choppers CH_1 and CH_2 separated by a distance L*

All contributions to the energy resolution in time-of-flight can be formulated as time uncertainty $\Delta t/t$. We consider only the primary spectrometer (before sample) and aim for an energy resolution better than 1µeV.

a) Show first that $\Delta E/E = 2\Delta t/t$ (express E as fct. of v and assume Δd =0):

$E =$___$\frac{1}{2} mv^2 = \frac{1}{2} m d^2/t^2$___and with $\Delta d = 0$:

$\Delta E =$ ___$-md^2/t^3\ \Delta t$___, which results in $\Delta E/E =$___$2\ \Delta t/t$___.

Several contributions add to the neutron flight time uncertainty Δt. To simplify, let's consider a chopper spectrometer with flight path L between two choppers as sketched in the Figure. I1. and let's first look at neutrons flying parallel to z.

b) Calculate the flight time along path L = 100 m: $T_0 \sim$ __0.159__ s.

If we want to get an energy resolution of 1µeV, this corresponds to

$\Delta E/E \sim$ __4.8×10^{-4}__ for 6.3Å neutrons.

This can give us an idea for the maximum allowed flight time difference along L:

$\Delta E/E_0 * T_0/2 \sim$ _____ __38__ _____ µsec

c) Path difference in neutron guide

For the reflected neutrons estimate the max. flight path differences in a super-mirror guide with m=2 coating and width w. The critical angle α (maximal reflection angle = half divergence) in such a guide is $\alpha \sim 0.1° \, m \, \lambda =$ __1.26__ °.

Estimate the flight path difference with respect to neutrons which fly parallel. One way is to show that $\Delta L/L = (1/\cos \alpha) - 1$ and thus:

$\Delta L/L =$ __2.4×10^{-4}__ $= \Delta t/t$ and therefore:

$\Delta E/E \sim$ __4.8×10^{-4}__.

We prove this by referring to Figure I1:

$l =$ __$w/\tan \alpha$__;

$l_a =$ __$w/\cos \alpha$__;

$l_a / l =$ _____ __$1/\cos \alpha$__ _____ independent of w; if n is the number of

reflections, then we can write the full path difference as:

$\Delta L = n*(l_a - l) =$ __$(L / l)*(l_a - l) = L(1/\cos\alpha - 1)$__ and thus $\Delta L/L = (1/\cos \alpha)-1$.

d) Chopper Opening Time

Another contribution is the chopper opening time which leads to a spread in neutron velocity and thus to flight time differences dt. In order to reach similar $\Delta t/t = \Delta v/v$ as above one needs fast rotating choppers delivering short pulses.

If CH1 releases at t = 0 an arbitrarily sharp pulse of a white beam, then the CH2 delay T selects a neutron velocity v_0 and the CH2 opening time determines $\Delta v/v$.

We want again 1µeV energy resolution therefore we need

$\Delta v/v_0 = \Delta t/T =$ __2.4×10^{-4}__.

The chopper opening time must then be

$\Delta t_{CH2} < 1/2*(1\mu eV/E_0)*/v_0 =$ __3.8×10^{-7}__ [s/m] * L [s].

Mechanically, the chopper opening time is defined as: $\Delta t_{CH2} = \beta / 360 / f$, where β is the chopper window angular opening and β/360 is the duty cycle (which equals the

fraction of neutrons transmitted by the chopper). We see that this condition can be achieved by increasing the flight path (or by decreasing v_n), by increasing the chopper frequency or by narrowing the chopper window (intensity loss).

Choosing a duty cycle of 0.01 one needs a very long flight path between CH1 and CH2 of L=100m and a high chopper frequency of __263__ Hz = __15790__ rpm to reach 1µeV energy resolution.

This condition becomes more restrictive if we consider the finite opening time of the first chopper as well. Finally, we mention that all the contributions in the primary and secondary spectrometer have to be added in quadrature:

$\Delta t/t = sqrt[(\Delta t_1/t_1)^2+(\Delta t_2/t_2)^2+.......]$

Additional choppers are usually needed to avoid frame overlap and harmonics, which reduces the intensity further. To achieve a 1µeV energy resolution by TOF is technically demanding (choppers), expensive (guides) and low in flux. Thus TOF-chopper-instruments have typically energy resolutions > 10 µeV. ex.: IN5 at 6.3Å has roughly 40 µeV energy resolution.

Increasing λ helps but reduces the maximum Q. Calculate the elastic Q for 3Å, 6Å and 15Å neutrons, assuming a maximum scattering angle of 140°:

$Q =$ ___$4\pi \sin\theta / \lambda$___ = __3.94__ Å^{-1}, __1.97__ Å^{-1} and __0.98__. Å^{-1}

I2. - Backscattering spectroscopy

Reactor backscattering spectrometers are based on perfect crystal optics. High energy resolution is achieved by choosing Bragg angles Θ as close as possible to 90°. Two major terms determine then the energy resolution: the spread in lattice spacing $\Delta d/d$ of the monochromator and the angular deviation ε from backscattering direction (the latter includes the beam divergence α if considered as $\varepsilon = \alpha/2$).

Write down the Bragg equation (neglecting higher orders): ___$\lambda = 2d \sin\theta$___ or equivalently using k=2π/λ and $\tau = 2\pi$/d (reciprocal lattice vector of the Bragg reflection): __$k = \tau / (2 \sin\theta)$__.

Deduce the wavelength resolution $\Delta\lambda/\lambda$ by differentiating the Bragg equation:

$\Delta\lambda =$ ___$2 \sin\theta.\Delta d$___ + ___$2d \cos\theta.\Delta\theta$___ and thus

$\Delta\lambda/\lambda =$ ___$\Delta d / d$___ +___$\cot\theta.\Delta\theta$___ , or equivalently:

$\Delta k=$ ___$\Delta\tau / (2 \sin\theta)$___ + ___$\{\tau / (2 \sin^2 \theta)\}\cos\theta.\Delta\theta$___ and thus

$\Delta k/k=$ __$\Delta\tau / \tau$__ + ___$\cot\theta.\Delta\theta$___.

The energy resolution is given by two terms. The first one, $\Delta d/d = \Delta\tau/\tau$, can be calculated by dynamical scattering theory as $\Delta\tau/\tau = h^2/m\, 4\, F_\tau\, N_c$, where F_τ is the structure factor of the reflection used and N_c the number density of atoms in the unit cell. The second one, the angular deviation, can for $\theta \approx 90°$ be expanded in powers of θ and contributes approximately as $\Delta\lambda/\lambda \sim \Delta\theta^2/4$ ($\Delta\theta$ in radians).

Calculate now the contribution to the energy resolution of both terms for a perfect crystal Si(111) monochromator (6.271Å, but approximate by 6.3Å as above).

With $F_{\tau=(111)}$ and N_c for Si(111) the extinction contribution for Si(111) in backscattering is $\Delta d/d = 1.86\ 10^{-5}$ and thus $\Delta E/E = \underline{\quad 3.46 \times 10^{-5} \quad}$ and $\Delta E = \underline{\,0.07\,}$ µeV.

Estimate the energy resolution contribution due to deviation from backscattering:

1) given by a sample diameter of 4 cm in 2 m distance from the analyser.

$\Delta E/E = \underline{\quad 5 \times 10^{-5} \quad}$, $\Delta E = \underline{\,0.1\,}$ µeV

2) given by this sample at 1m distance:

$\Delta E/E = \underline{\quad 2 \times 10^{-5} \quad}$, $\Delta E = \underline{\,0.42\,}$ µeV

3) given by a detector being placed near backscattering, a sample - analyser distance of 1m and the distance sample center - detector center = 10cm below the scattering plane; the focus of the analyser sphere is placed in the middle between sample and detector:

$\Delta E/E = \underline{\quad 1.25 \times 10^{-3} \quad}$. $\Delta E = \underline{\,2.6\,}$ µeV

These examples show that for small enough deviations from BS energy resolutions of < 1µeV are easily achievable. Comparing this to TOF contributions above, it becomes clear that for a spallation source backscattering instrument, which combines TOF in the primary spectrometer with near-BS in the secondary spectrometer, it is very difficult to achieve sub-µeV resolution. The SNS backscattering (BASIS) instrument with 80m flight path has for example an energy resolution for Si(111) of 2.5 µeV.

I3. - Neutron spin-echo spectroscopy

In neutron spin echo one uses the neutron spin which undergoes precessions in a magnetic field B. The precession angle φ after a path length L depends on the field integral, given by $\varphi = \gamma * B * L / v_n$ (γ = gyromagnetic ratio of the neutron, v_n = neutron speed). For a polychromatic beam the precession angles of the neutron spins will be very different depending on the neutron speed and thus a previously polarized beam becomes depolarized. The trick is then to send the neutrons after the sample through a field with opposite sign and with the same field integral. Therefore, for elastic scattering, the precessions are "turned backwards", again depending on the neutron velocity, and the full polarization is recovered. This allows the use of a wide

wavelength band (range of incident neutron speeds) and therefore a high intensity which is 'decoupled' from the energy resolution.

In order to estimate a typically achievable energy resolution, we can calculate the longest time which is easily accessible in NSE.

The NSE time is given by: $t_{NSE} = \hbar\gamma \, BL / (m_n \, v_n^3)$ thus it is proportional to the largest achievable field integral B*L, which we take as 0.25 [T*m].

Calculate the longest NSE time t_{NSE} for λ=6.3Å neutrons (use v_n calculated above), knowing that $\gamma = 1.832 \, 10^8$ [$T^{-1} \, s^{-1}$] , $\hbar$= 1.054*10^{-34} J s; and m_n= 1.675*10^{-27} kg:

t_{NSE} = ___11.7___ ns.

Convert this time into an energy by multiplying its reciprocal value with

h=4.136 µeV ns; we get: E_{NSE}= ___0.35___ µeV.

For comparing measurements in time and in energy one often refers to Fourier-transformation which relates e.g. the characteristic relaxation time τ of an exponential relaxation in time to the width of a Lorentzian function in energy by $\tau = 1/\omega$. In spite of the fact that the relaxation time is usually smaller than the longest NSE time, converting the corresponding energy resolution by this relation gives:

E_τ = ___0.056___ µeV .

Because of $\tau < t_{NSE}$ and also because energy spectrometers can usually resolve better than the HWHM, the comparable resolution energy lies somewhere in between the two values calculated.

Note that the longest NSE time depends on wavelength λ as $t_{NSE} \propto$ __λ^3__. Thus the resolution improves fast for increasing λ, but like calculated for the other spectrometers above, the maximum Q is reduced.